# A high-overtone bulk acoustic wave resonator-oscillator-based 4.596 GHz frequency source: Application to a coherent population trapping Cs vapor cell atomic clock

Thomas Daugey, Jean Friedt, Gilles Martin, Rodolphe Boudot

▶ **To cite this version:**

Thomas Daugey, Jean Friedt, Gilles Martin, Rodolphe Boudot. A high-overtone bulk acoustic wave resonator-oscillator-based 4.596 GHz frequency source: Application to a coherent population trapping Cs vapor cell atomic clock. Review of Scientific Instruments, 2015, 86 (11), pp.114703. 10.1063/1.4935172 . hal-01232007

**HAL Id: hal-01232007**
**https://hal.science/hal-01232007**

Submitted on 19 Apr 2021

**HAL** is a multi-disciplinary open access archive for the deposit and dissemination of scientific research documents, whether they are published or not. The documents may come from teaching and research institutions in France or abroad, or from public or private research centers.

L'archive ouverte pluridisciplinaire **HAL**, est destinée au dépôt et à la diffusion de documents scientifiques de niveau recherche, publiés ou non, émanant des établissements d'enseignement et de recherche français ou étrangers, des laboratoires publics ou privés.

Distributed under a Creative Commons Attribution 4.0 International License

# A high-overtone bulk acoustic wave resonator-oscillator-based 4.596 GHz frequency source: Application to a coherent population trapping Cs vapor cell atomic clock

Thomas Daugey, Jean-Michel Friedt, Gilles Martin, and Rodolphe Boudot
*FEMTO-ST, CNRS, UFC, 26 chemin de l'Epitaphe 25030 Besançon Cedex, France*

(Received 13 August 2015; accepted 21 October 2015; published online 11 November 2015)

This article reports on the design and characterization of a high-overtone bulk acoustic wave resonator (HBAR)-oscillator-based 4.596 GHz frequency source. A 2.298 GHz signal, generated by an oscillator constructed around a thermally controlled two-port aluminum nitride-sapphire HBAR resonator with a Q-factor of 24 000 at 68 °C, is frequency multiplied by 2–4.596 GHz, half of the Cs atom clock frequency. The temperature coefficient of frequency of the HBAR is measured to be −23 ppm/°C at 2.298 GHz. The measured phase noise of the 4.596 GHz source is −105 dB rad$^2$/Hz at 1 kHz offset and −150 dB rad$^2$/Hz at 100 kHz offset. The 4.596 GHz output signal is used as a local oscillator in a laboratory-prototype Cs microcell-based coherent population trapping atomic clock. The signal is stabilized onto the atomic transition frequency by tuning finely a voltage-controlled phase shifter implemented in the 2.298 GHz HBAR-oscillator loop, preventing the need for a high-power-consuming direct digital synthesis. The short-term fractional frequency stability of the free-running oscillator is $1.8 \times 10^{-9}$ at one second integration time. In locked regime, the latter is improved in a preliminary proof-of-concept experiment at the level of $6.6 \times 10^{-11}\ \tau^{-1/2}$ up to a few seconds and found to be limited by the signal-to-noise ratio of the detected CPT resonance. © *2015 AIP Publishing LLC.* [http://dx.doi.org/10.1063/1.4935172]

## I. INTRODUCTION

Over the last decade, outstanding progress in micro-electromechanical systems (MEMS) technologies and semiconductor lasers, combined to coherent population trapping (CPT) physics,[1,2] has allowed the development of high-performance miniature atomic clocks (MACs) that combine a volume of about 15 cm$^3$, a total power consumption lower than 150 mW and a fractional frequency stability lower than $10^{-11}$ at 1 h and 1 day integration time.[3–5] Such frequency references, now commercially available,[6] can provide the base for a number of mobile and embedded applications including network synchronization, new-generation mobile telecommunication systems, satellite-based navigation systems on-earth receivers, secure banking data transfer or military and avionic systems. In a Cs atom-based MAC, a 4.596 GHz local oscillator (LO), ultimately frequency-stabilized onto the atomic clock transition frequency, is required to drive a vertical-cavity-surface-emitting laser (VCSEL).

This local oscillator needs to satisfy numerous stringent requirements. It must be integrated onto a reduced surface footprint (<1 cm$^2$), consume a negligible maximum power of about 50 mW for battery-powered applications, deliver an output microwave power tunable between −6 and 0 dBm[7,8] to drive the VCSEL laser and be compatible with low-cost mass production. The LO output frequency must be tunable with a high resolution so that the relative frequency error remains significantly smaller than the targeted clock stability. In general, a frequency resolution at the mHz level is desired to ensure a frequency stability below $10^{-12}$. Additionally, the output 4.596 GHz signal must be modulated in frequency with a rate and a depth of about 1 kHz in order to be used in a lock-in amplifier configuration. Moreover, phase noise is critical because the short term frequency stability of a passive atomic frequency standard can be degraded by the LO phase noise through an intermodulation effect.[9,10] The fractional frequency stability limitation $\sigma_{y_{LO}}(\tau)$ of the atomic clock due to this aliasing effect can be approximated by

$$\sigma_{y_{LO}}(\tau = 1\ \mathrm{s}) \sim \left(\frac{f_m}{\nu_0}\right)\sqrt{S_\varphi(2f_m)}, \tag{1}$$

where $S_\varphi(2f_m)$ is the power spectral density (PSD) of the LO phase fluctuations in the free-running regime at Fourier frequency $f = 2f_m$ and $\tau$ the averaging time. According to this relation, assuming a LO modulation frequency $f_m$ of 1 kHz and targeting $\sigma_{y_{LO}} < 2 \times 10^{-11}$ at 1 s integration time, we calculate that $S_\varphi(2f_m = 2\ \mathrm{kHz})$ must be lower than −77 dB rad$^2$/Hz.

The most common technological approach for the development of a LO in MAC application, using discrete components, consists of a frequency synthesizer using a LC voltage-controlled oscillator (VCO) phase-locked to a 10 MHz quartz oscillator through a fractional-N phase-locked loop (PLL). In Ref. 5, a 4.596-GHz synthesizer was built reaching a power consumption of 40 mW and giving a clock short-term stability of $5 \times 10^{-11}\ \tau^{-1/2}$, limited by the RF synthesizer phase noise. In Ref. 11, a 12-mW single-chip 4.596 GHz frequency synthesizer ASIC implemented in a 130-nm RF CMOS process was developed for a Cs MAC, demonstrating a clock stability of $5 \times 10^{-11}$ at 1 s, limited by the signal-to-noise ratio of the detected CPT signal. However, in such systems, the frequency multiplication degrades the phase noise and can consume up to 50% of the MAC total power budget.[5] In an another way, Brannon *et al.* developed for MAC applications microwave

 © 2015 AIP Publishing LLC

oscillators based on quarter-wavelength ceramic-filled coaxial resonators. Nevertheless, these sources exhibited modest phase noise performances of −62 dB rad$^2$/Hz and −94 dB rad$^2$/Hz at 1 kHz and 10 kHz from the carrier, respectively.[7]

A promising alternative solution for MAC applications is the development of microwave MEMS oscillators based on bulk acoustic wave (BAW) resonators. These resonators exhibit an extremely small size and power consumption, very high Q × f products[12] up to $10^{14}$ and high-potential for wafer-level fabrication. In this domain, High-overtone Bulk Acoustic Resonators (HBARs) have emerged as a valuable tradeoff between thin-film bulk acoustic resonators (FBARs)—reaching the microwave frequency range but requiring a thin and fragile membrane to be fabricated—and Surface Acoustic Wave (SAW) resonators that benefit from a mature technology level, advanced design tools, simpler manufacturing steps compared to thin-film-based devices but whose operating frequency is limited by lithography resolution. Numerous HBAR-based oscillators have been developed (see, for example, Refs. 13–17). However, because of the difficulty to tune the LO frequency to the exact atomic transition frequency, we found a unique example in the literature of a HBAR-based oscillator frequency-locked to a CPT resonance. In 2009, Yu *et al.* demonstrated a HBAR-based 3.6 GHz Pierce oscillator with a phase noise of −77 dB rad$^2$/Hz at 1 kHz Fourier frequency, a power consumption of 3.2 mW, a frequency stability of $1.5 \times 10^{-9}$ at 1 s[17] in free-running regime and claimed to be improved at the level of $1 \times 10^{-10}$ when locked to a cm-scale Rb vapor cell. Note that in this reference, the output signal of the HBAR oscillator was mixed with a RF signal from an external synthesizer, highlighting the difficulty to tune the output frequency to the exact atomic transition frequency. Moreover, a vapor cell with cm-scale dimensions was used in the CPT experiment. Also, no figures were reported on the CPT clock experiment in this article.

This article reports on an original double-port aluminium nitride (AlN)/Sapphire 2.298 GHz HBAR-oscillator-based 4.596 GHz frequency synthesizer used as a local oscillator in a Cs vapor-microcell based CPT atomic clock. While not fully integrated, the system architecture presented in this work is found to be well suitable for MAC applications with high potential for miniaturization and low power consumption. Dedicated design rules, "juggling" with the resonator dimensions, materials, temperature sensitivity, and multi-mode spectrum specificity of HBAR, are provided for the resonator to be best suited to this application and to ensure the output frequency to be resonant with Cs atom at 4.596 GHz. Section II describes the resonator. Section III describes the HBAR-based 2.298 GHz oscillator and 4.596 GHz frequency synthesizer. Section IV details the CPT experiment using the HBAR-based frequency source.

## II. THE HBAR RESONATOR

A HBAR is obtained by stacking a thin piezoelectric film over a low-acoustic loss substrate. The thin piezoelectric film generates an acoustic wave by converting an incoming exciting electrical signal, while the thick substrate confines the acoustic energy, allowing for high quality factor. This coupled resonant structure yields a complex multimode spectrum with a comb of equally spaced modes, with a frequency interval defined by the acoustic velocity in the substrate divided by the substrate thickness. The admittance of these modes is modulated by a broad envelope, whose maximum is defined by the thin film resonance frequency and its overtones.

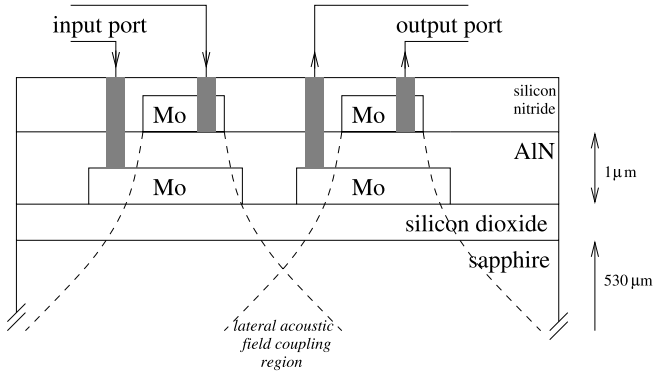


FIG. 1. Schematic cross section of the 2-port laterally coupled HBAR. The filled rectangles (grey) indicate Ni-Au filled vias, while the dashed line hints at the acoustic field distribution for defining the region of lateral acoustic field coupling between the two transducers.

Figure 1 shows the architecture of the HBAR resonator. The approach, inspired by Refs. 18 and 19, is to build two single-port HBAR resonators close enough to one another in order to promote acoustic coupling via evanescent waves by proper selection of material combinations. The bottom electrode is shared by the two resonators and is accessed through dedicated vias connected to ground. Typical losses are in the 15–20 dB range, with a dynamic range between resonance and baseline better than 15 dB. This double-port resonator configuration is of great interest to simplify the development of an oscillator. Unlike the negative resistance Clapp, Pierce, or Colpitts oscillators which use the anti-resonance of single-port resonators, dual-port resonator oscillators allow a rational approach of Barkhausen conditions. Additionally, the double-port configuration is less sensitive to parasitic electrical elements than standard oscillator architectures (Colpitts, Clapp, or Pierce).

Five degrees of freedom are available when designing an HBAR: piezoelectric thin film and low acoustic loss substrate material properties, thicknesses, and electrode geometry. The piezoelectric substrate is selected with a high coupling coefficient for each mode to be well defined, since each piezoelectric layer overtone spreads its coupling coefficient over all the modes of the comb included in each envelope. Here, a thin film of AlN is deposited under vacuum. The low-acoustic loss substrate defines each mode $Q$-factor: the lower the losses, the better the quality factor. Here, sapphire is selected for its excellent properties in the microwave frequency range.[20]

The resonance frequency $f_p$ of the piezoelectric film fundamental mode is fixed by the ratio $c_p/t_p$ with $c_p$ the longitudinal wave velocity in the piezoelectric substrate and $t_p$ the piezoelectric film thickness. Here, considering the addition of Mo electrodes, a longitudinal wave velocity $c_p$ of 11 270 m/s in AlN and a reached thickness $t_p$ of about 1 $\mu$m,

the frequency of the fundamental mode is $f_p = c_p/(2 \cdot t_p) \simeq 1.25$ GHz. Consequently, the second overtone is used to reach the frequency of $2f_p \simeq 2.5$ GHz, close to the quarter of the Cs clock frequency (2.298 GHz). The choice of the substrate thickness that defines the spacing between adjacent modes results from several key points. On the one hand, the thinner the substrate, the wider the spacing and the easier the oscillator design for selecting the targeted mode, but the more fragile the resonator. Obviously, without any other freedom degrees such as the resonator temperature, an excellent manufacturing resolution on the substrate thickness would be required in order to tune finely the resonator frequency to the exact atomic transition frequency. In a miniature Cs vapor cell clock, the CPT resonance linewidth ranges from a few kHz to 20 kHz. This order of magnitude determines the required resolution $\delta f$ on the HBAR resonance position accuracy. Let us assume a targeted operation frequency of about 4 GHz and a mode spacing of about 10 MHz as justified later. The overtone number would be $N = 400$. Assuming that the piezoelectric layer acts as an acoustic energy pump and that the mode frequency is governed by the substrate, the uncertainty $\delta t_s$ on the substrate thickness $t_s$ is given by

$$\delta t_s = \frac{N \times c_s}{2 \times f_0^2} \times \delta f,$$

with $c_s \simeq 10^4$ m/s the acoustic wave velocity in the substrate. We calculate that reaching a frequency uncertainty $\delta f$ below 20 kHz requires a control of the substrate thickness such as $\delta t_s \simeq 2.5$ nm that is not achievable with our technology.

Therefore we decided to adopt a two-step tuning strategy of the HBAR-based oscillator to ensure the output signal to be resonant with Cs atoms. A first coarse frequency tuning is reached by exploiting the frequency-temperature dependence of the HBAR. A second fine frequency tuning over a few tens of kHz is achieved by tuning the bias point of a voltage controlled phase shifter (VCPS) in the oscillator loop (see Section III). The latter tuning capability must be used cautiously since the multi-mode nature of the resonator induces frequency jumps if the VCPS bias point is changed so that an adjacent mode is favored.

Figure 2(a) displays for a wide span of 4 GHz the measured $S_{21}$ parameter (magnitude in dB) of the HBAR-resonator. The multi-modal structure of the HBAR is clearly shown. Zooming in the 2.298 GHz region, modes that can be used for the present Cs vapor cell atomic clock application are highlighted. A 100-MHz wide bandpass SAW filter (Golledge TA0700A) of central frequency 2.25 GHz is used for primary modal selection. In the filter bandwidth, about ten modes of the resonator response are selected and can be used for oscillation. Figure 2(b) shows the spectrum ($S_{21}$ parameter, magnitude in dB) of the mode selected for the oscillator loop. Resonance and anti-resonance are well observed. Due to the double-port configuration, the resonance mode is found to be split into two neighbour distinct modes. For a resonator temperature of 55 °C, insertion losses are measured to be about 17 dB. The resonance quality-factor $Q$, defined as $Q = \frac{\nu_0}{\Delta\nu}$ where $\nu_0$ is the resonance frequency and $\Delta\nu$ the 3-dB bandwidth, is measured to be 24 200.

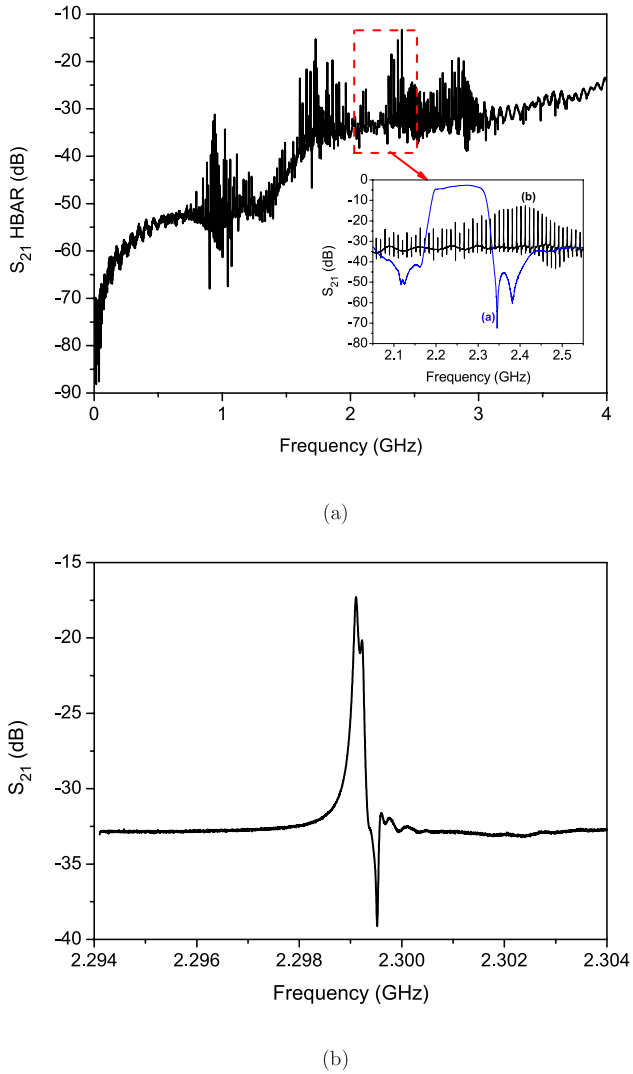


FIG. 2. (a) $S_{21}$ parameter (magnitude) of the HBAR resonator over a large span of 4 GHz. The inset shows a zoom from 2.05 to 2.55 GHz. In the inset, the blue line (a) plots the transfer function of the SAW filter used to select a reduced number of acoustic modes. The other curve shows the response of the HBAR. (b) Selected resonance mode of the HBAR resonator at about 2.298 GHz. The HBAR temperature here is 55 °C. The Q-factor is measured to be 24 200.

Figure 3 shows the evolution of the HBAR frequency and Q-factor versus the resonator temperature in the 30–80 °C range. The temperature coefficient of frequency (TCF) of the resonator is measured to be −23.1 ppm/°C, i.e., −53.3 kHz/°C. We measured that the resonator Q-factor does not change significantly in this temperature range.

The temperature sensitivity of −53.3 kHz/°C helps to define here the substrate thickness. Considering that we wish to keep the resonator below a temperature of 220 °C, the temperature span from room temperature to the maximum operating temperature is about 200 °C. Thus, the tuning capability of the frequency of each mode is 10.66 MHz and dictates the mode spacing. In our case, the mode spacing defined by a sapphire substrate of thickness $t_s = 530$ $\mu$m[21] propagating a wave at a velocity $c_s = 11\,000$ m/s[22] is $c_s/t_s/2 = 10$ MHz. Consequently, the HBAR is always able to bring one of its mode at 2.298 GHz, quarter of the Cs microwave transition.

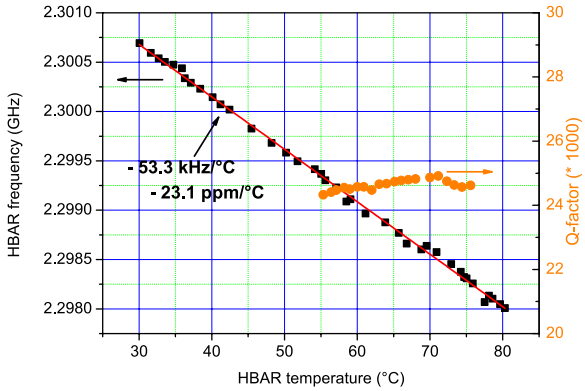


FIG. 3. HBAR frequency (filled squares, left axis) and loaded Q-factor (filled circles, right axis) versus the resonator temperature. Frequency measurement data are fitted by a linear function (solid line) with a slope of −53.3 kHz/ °C.

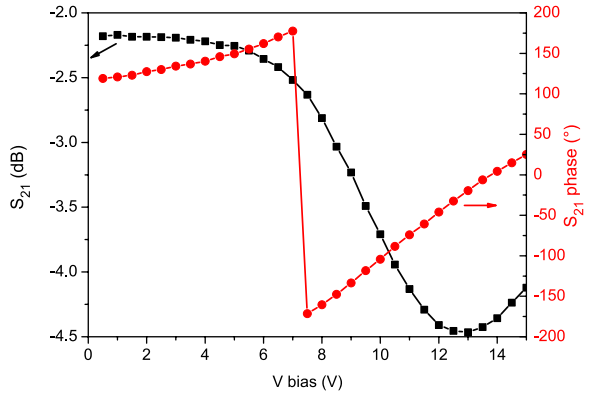


FIG. 5. Response ($S_{21}$ parameter) of the VCPS versus the control bias voltage. Filled squares, left axis: magnitude in dB. Filled circles, right axis: phase (°).

## III. THE HBAR-OSCILLATOR

Figure 4 shows the oscillator loop constructed around the two-port HBAR resonator. The resonator is stabilized at 68 °C with a high-precision temperature controller described in Ref. 23. At this temperature, insertions losses of the resonator are about 17 dB and the Q-factor is 24 200.

Two sustaining amplifiers (Mini-circuits ZX60-3011+ and ZX60-3018G-S+), with a total gain of 30 dB, are used to compensate losses of the circuit after selecting the 10 modes around 2.25 GHz with the Golledge TA0700A bandpass filter. The total amplification stage, exhibiting a measured residual flicker phase noise of −120 dB rad$^2$/Hz at 1 Hz offset frequency, is not specifically low-phase noise but rather wideband, meeting the flexibility requirement of selecting the appropriate HBAR resonance.

A phase shifter is implemented to tune the correct phase needed to meet the Barkhausen condition required for oscillation. A VCPS (Minicircuits JSPHS2484) is implemented in the loop. This VCPS is used for fine tuning of the oscillator loop phase and consequently of the local oscillator output frequency. Figure 5 exhibits the $S_{21}$ parameter (magnitude in dB and phase) versus the control bias voltage. The VCPS is operated around a bias voltage set point that allows to obtain a high voltage-to-phase (in °/V) dependence.

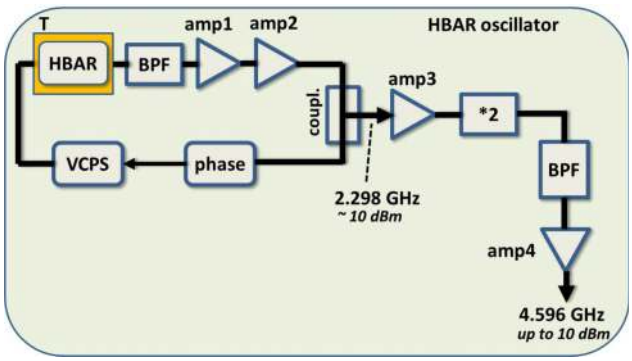


FIG. 4. Architecture of the HBAR-based 2.298 GHz oscillator loop and frequency multiplication chain to generate an output 4.596 GHz signal. Amps 1, 2, 3, and 4 are microwave amplifiers. BPFs are band-pass filters. VCPS: voltage-controlled phase shifter, phase: variable phase shifter, coupl.: coupler, ×2: frequency doubler. References of the components are given in the text.

Simultaneously, it should be preferred to operate the VCPS at a bias voltage where insertion losses of the VCPS are small to sustain oscillation and where the induced residual amplitude modulation is reduced. In our experiment, the chosen set point was close to 6 V. Around this value, the tuning voltage-frequency sensitivity was measured to be 8 kHz/V.

The useful 2.298 GHz output signal of the HBAR-based oscillator loop is extracted using a microwave coupler (Mini-circuits MC ZABDC20-252-S+). This signal is then amplified with a microwave amplifier (Minicircuits ZX60-8008E-S+) and frequency-multiplied to 4.596 GHz with a low noise frequency doubler (Mini-circuits ZX90-2-36S+). The 4.596 GHz signal is bandpass-filtered with a 50-MHz bandwidth bandpass filter and amplified again to a power up to 10 dBm with an amplifier (Minicircuits ZX60-8000E-S+). A variable attenuator is used at the output to adjust the microwave power that drives the VCSEL laser. Figure 6 shows the spectrum of the 4.596 GHz output signal measured with a spectrum analyzer.

Figure 7 shows the absolute phase noise of the HBAR-based oscillator 2.298 GHz signal and the output 4.596 GHz signal, respectively. For comparison, these phase noise performances are compared to those of a low-power consumption (12 mW) 4.596 GHz frequency synthesizer ASIC developed in Ref. 11 for MAC applications, and to those of a low power 4.596 GHz frequency synthesizer developed in Ref. 5. Also,

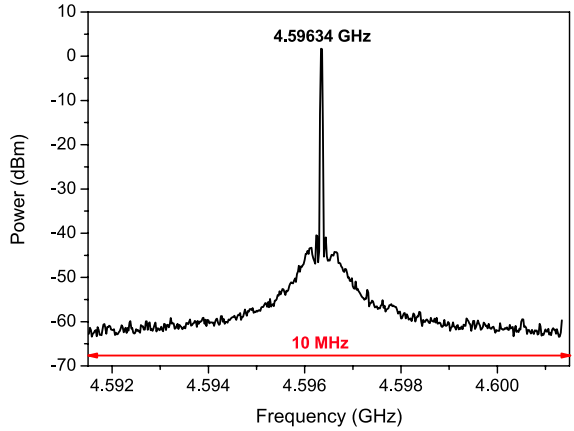


FIG. 6. Output spectrum of the 4.596 GHz signal over a 10 MHz span measured with a microwave spectrum analyzer. RBW, VBW: 30 kHz.

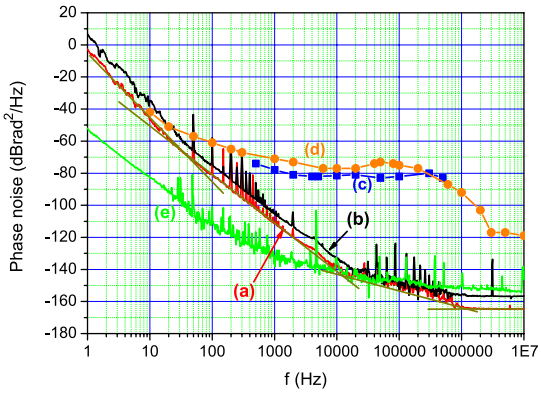


FIG. 7. Absolute phase noise performances. (a) HBAR-based oscillator 2.298 GHz signal, (b) HBAR-based synthesizer output 4.596 GHz signal, (c) 4.596 GHz synthesizer ASIC developed in Ref. 11, (d) 4.596 GHz synthesizer used in the commercially available CSAC SA-45 from Microsemi, (e) state-of-the-art 100 MHz OCXO ideally reported to 4.596 GHz.[24] Solid lines at 2.298 GHz are used to extract $b_i$ coefficients of the phase noise spectrum power-law such as $S_\varphi(f) = \sum_{i=0}^{-4} b_i f^i$.

phase noise performances of a state-of-the-art 100 MHz oven-controlled quartz-crystal oscillator (Pascall OCXOF-E-100) ideally reported to 4.596 GHz are given.[24] The phase noise spectrum of the free-running 2.298 GHz signal is measured to be −112, −140, and −164 dB rad$^2$/Hz at 1 kHz, 10 kHz, and 1 MHz offset frequencies, respectively. For $f < 20$ Hz, a $f^{-4}$ slope is obtained, attributed to the temperature sensitivity of the oscillator frequency. We observed that the measured oscillator phase noise in the flicker frequency region ($f^{-3}$ slope) is about 5 dB higher than the oscillator phase noise expected by the Leeson effect.[25] Two reasons are mainly suspected to explain this discrepancy. The first reason is a possible non-linear behavior of the HBAR resonator with input power or impedance matching, yielding that the resonator loaded Q-factor in actual oscillator loop conditions would be lower than the one measured in Fig. 2(b) in open-loop conditions with the network analyzer.[26] The second possible reason could be that the oscillator phase noise is limited by the residual phase noise of the HBAR resonator.[26–28] Further studies are in progress for better understanding. Additionally, note that the excess level of noise on the oscillator phase noise spectrum in the 20 kHz–800 kHz offset frequency range is attributed to the signal source analyzer (Agilent E5052B).

Due to the multiplication factor by 2, the absolute phase noise of the 4.596 GHz is found to be 6 dB higher, except for the phase noise floor that is limited by the residual noise of the by-2 multiplication chain to −157 dB rad$^2$/Hz. The phase noise of the 4.596 GHz signal is measured at the level of −105 dB rad$^2$/Hz for an offset frequency $f = 1$ kHz. Compared to the 4.596 GHz synthesizer ASIC developed in Ref. 11, phase noise performances of the present HBAR-based source are 26 dB and 67 dB better for $f = 1$ kHz and $f = 100$ kHz, respectively. Compared to the 100-MHz OCXO-based synthesizer, phase noise performances of the HBAR-based source are found to be 25 dB worse for $f = 1$ kHz and 5 dB better for $f = 1$ MHz, respectively. This demonstrates the high potential of HBARs for the development of ultra-low phase noise microwave sources, with high potential for low power consumption and miniaturization.

For information, according to Eq. (1), using the present HBAR-based frequency source and assuming $f_m = 1$ kHz, the Dick effect contribution to the clock fractional frequency stability $\sigma_{y_{LO}}(\tau = 1\text{ s})$ is rejected at the level of $4.3 \times 10^{-13}$. This remarkable value is close to the ultimate atomic clock quantum noise limit for microcell-based miniature CPT atomic clocks.[29]

## IV. CPT ATOMIC CLOCK EXPERIMENT

### A. Description

In a Cs CPT MAC, Cs atoms confined in a miniature vapor cell interact in a so-called lambda-scheme with a resonant bi-chromatic optical field generated by a laser system. When the frequency difference between both optical lines exactly equals the atomic ground state hyperfine splitting, atoms are trapped through a destructive quantum interference process into a coherent superposition of two long-lived ground state hyperfine levels. In this dark state, atoms are under ideal conditions fully decoupled from the excited state, resulting in an increase of the atomic vapor transparency. The resulting CPT resonance, whose linewidth is ultimately limited by the atom-light interaction time, can be used as a narrow frequency discriminator for the development of an atomic clock.

Figure 8 presents the Cs CPT clock experimental setup. The laser source is a 25 MHz-linewidth custom-designed VCSEL tuned at 894.6 nm on the Cs $D_1$ line.[30,31] The laser injection current is directly modulated at 4.596 GHz by a local oscillator to generate two phase-coherent first-order optical sidebands frequency-split by 9.192 GHz for CPT interaction. Two different microwave sources were tested for comparison. The first source is the HBAR-based frequency source described in this article. The second source is a commercially available microwave frequency synthesizer (Rohde-Schwarz RS SMB100A) driven by a high-stability 10 MHz quartz oscillator. The output laser beam is collimated with a collimation lens to reach a beam diameter of 2 mm, attenuated in power with a neutral density filter to a total laser power of about 30 $\mu$W and circularly polarized thanks to a quarter-wave plate. The bi-chromatic optical field interacts with Cs atoms confined in a micro-fabricated vapor cell whose architecture is described in Ref. 32. A Ne buffer gas with total pressure of about 113 Torr (at 84 °C) is used to increase the time for Cs atoms to reach the cell walls. In this so-called Dicke regime,[33] the Doppler effect is canceled and a narrow microwave CPT clock resonance of a few kHz can be detected. The presence of Ne buffer gas shifts the Cs atom clock frequency by about +78 kHz (referred to the unperturbed Cs atom frequency = 9.192 631 770 GHz). In the optical domain, the presence of buffer gas causes a broadening of optical transitions of about 10.85 MHz/Torr.[34] The microcell temperature is stabilized to within 1 m°C around 84 °C where the CPT signal height is maximized. The Cs-Ne cell is surrounded by a solenoid applying a static magnetic field of 10 $\mu$T in order to raise the Zeeman degeneracy and to isolate the hyperfine clock transition $|F = 3, m_F = 0\rangle \rightarrow |F = 4, m_F = 0\rangle$. The ensemble is inserted into a

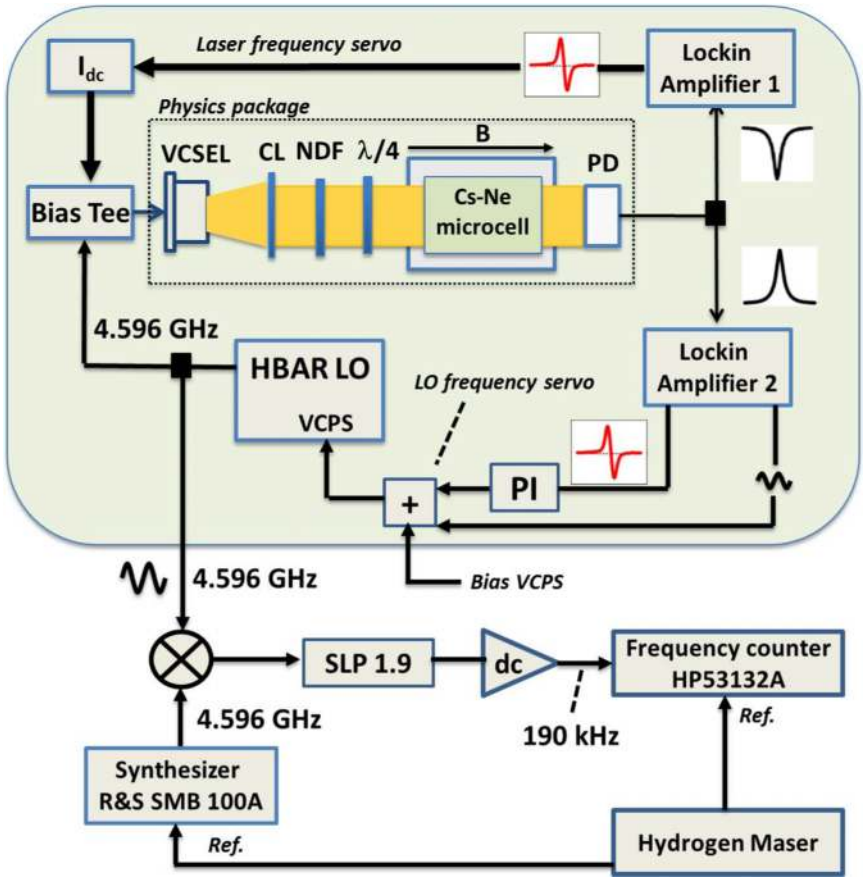


FIG. 8. Experimental setup of the CPT clock. A physics package contains the VCSEL laser, optics to shape and polarize the laser beam, a Cs-Ne microcell where CPT interaction takes place and a photodiode to detect the transmitted light through the cell. The VCSEL laser is modulated with a 4.596 GHz from the local oscillator. A bias-tee is used to drive the laser both with a DC current ($I_{dc}$) and the 4.596 GHz signal for modulation and optical sidebands generation. The output signal from the photodiode is used in two servo loops: laser frequency stabilization and local oscillator frequency stabilization. The local oscillator frequency is locked to the atomic transition frequency by correcting the VCPS bias voltage. The output 4.596 GHz from the HBAR-based frequency source is mixed with the 4.596 GHz signal from a reference microwave synthesizer (RS SMB100A) driven by a hydrogen maser. The 190 kHz beatnote is filtered and counted with a frequency counter. A PC, not shown here, allows to compute and evaluate Allan deviation from the counter data. CL: collimation lens, NDF: neutral density filter, $\lambda/4$: quarter-wave plate.

cylindrical mu-metal magnetic shield in order to prevent magnetic perturbations from the environment. The laser power transmitted through the cell is detected by a photodiode. The output signal of the photodiode is used in two main servo loops. The first servo loop aims to stabilize the laser frequency on the position of maximum optical absorption. For this purpose, the laser DC current is modulated (modulation frequency FM of 49 kHz) and the signal at the output of the photodiode is synchronously demodulated with the lockin-amplifier LA1 that generates a zero-crossing error signal. The latter is processed in a PI controller and used to correct with a bandwidth of a few kHz the laser current for stabilization of the laser frequency. The second servo loop is used to stabilize the local oscillator frequency onto the CPT clock resonance. Using the HBAR-based frequency source, the experimental procedure is as follows. First, the HBAR temperature is adjusted to about 68 °C to tune roughly the local oscillator frequency to the clock frequency. Second, the bias voltage of the VCPS is slowly swept with a ramp voltage to scan and detect the CPT resonance. Once the CPT resonance is detected, the bias voltage of the VCPS is sinusoidally modulated (FM = 932 Hz and modulation depth of 2.5 kHz) to modulate the LO frequency and the signal at the output of the photodiode is synchronously demodulated with the lockin-amplifier LA2. The zero-crossing error signal at the output of the lockin amplifier LA2 is processed in a PI controller and fed back to the VCPS bias voltage to stabilize the HBAR-source frequency to the CPT clock frequency.

The fractional frequency stability of the HBAR-based 4.596 GHz local oscillator is measured by beating it using a microwave mixer with the 4.596 GHz signal generated by a commercial microwave frequency synthesizer (Rohde-Schwarz RS SMB100A). The latter is driven by a reference hydrogen maser available in the laboratory. The 190 kHz beatnote is filtered using a 1.9 MHz low-pass filter, amplified with a low noise DC amplifier and counted by a frequency counter (HP53132A) referenced to the hydrogen maser. When using the 4.596 GHz RS SMB100A synthesizer as local oscillator of the clock, the correction signal is fed back to the 10 MHz quartz oscillator pilot. The output 10 MHz signal, locked to the atomic signal, is compared with a 10.190 MHz signal coming from a second commercial synthesizer driven by the hydrogen maser. This part is not shown in Fig. 8.

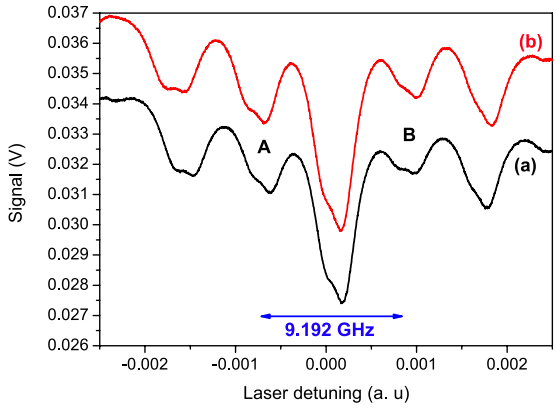


FIG. 9. Optical absorption lines detected by scanning the laser frequency. The VCSEL laser is modulated at 4.596 GHz (a) with the HBAR-based frequency source, (b) with the laboratory-prototype microwave synthesizer (RS SMB100A).

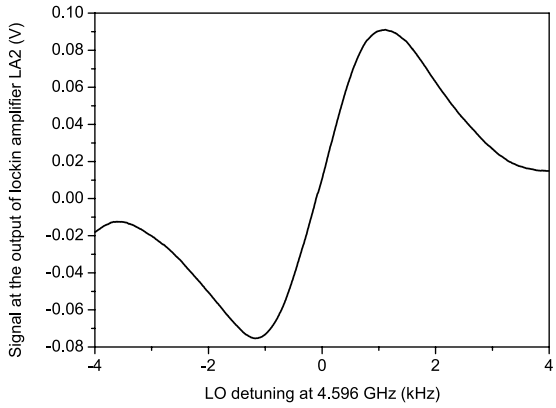


FIG. 10. CPT resonance (output of the lockin amplifier LA2) detected in the Cs-Ne microcell using the 4.596 GHz HBAR-based local oscillator.

## B. Experimental results

Figure 9 shows optical absorption lines detected at the output of the Cs-Ne cell by scanning the laser frequency. The laser frequency is modulated at 4.596 GHz by the local oscillator with a power of +3 dBm. Absorption lines detected with the HBAR-based frequency source (curve (a)) or the SMB100A frequency synthesizer (curve (b)) are compared. When the 4.596 GHz signal is not applied, only both absorption doublets separated by 9.192 GHz (noted A and B on Fig. 9) of the Cs $D_1$ line hyperfine structure are visible. Each absorption doublet is composed of two absorption peaks separated by 1.16 GHz (frequency separation between both energy levels of the Cs $D_1$ line excited state) that here are not well-resolved because of the buffer-gas induced optical broadening effect. When the 4.596 GHz modulation signal is applied, optical sidebands are generated and the effect of the 4.596 GHz modulation is clearly visible. In this case, both initial absorption doublets combine into a central doublet with amplitude that increases with increased microwave power. At the end, the microwave power is fixed at +3 dBm where the CPT signal is maximized. Similar absorption spectra are obtained with the HBAR-based frequency source or the high-performance commercial microwave synthesizer for same microwave power.

Figure 10 displays the CPT clock signal detected at the direct output of the lockin amplifier LA2 when the HBAR-based source frequency is slowly scanned around 4.596 354 GHz. We extract from this figure that the CPT resonance linewidth $\Delta\nu$ at 9.192 GHz is about 7 kHz. The frequency discriminator slope at the output of the lockin-amplifier is $8.2 \times 10^{-5}$ V/Hz.

Figures 11(a) and 11(b) show, respectively, the local oscillator frequency versus time and corresponding Allan deviation versus the averaging time $\tau$. Different configurations were tested: free-running HBAR-based local oscillator without temperature control of the HBAR resonator (a), free-running HBAR-based local oscillator with temperature control of the HBAR resonator (b), HBAR-based local oscillator with HBAR temperature control and locked to the atoms (c), SMB100A synthesizer-based local oscillator locked to the atomic transition (d). Without HBAR temperature stabilization, the

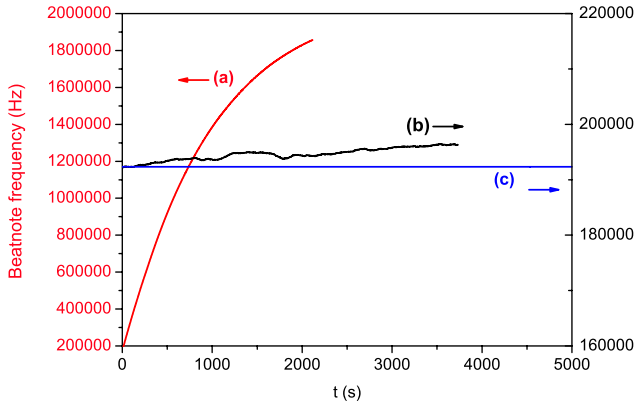


(a)

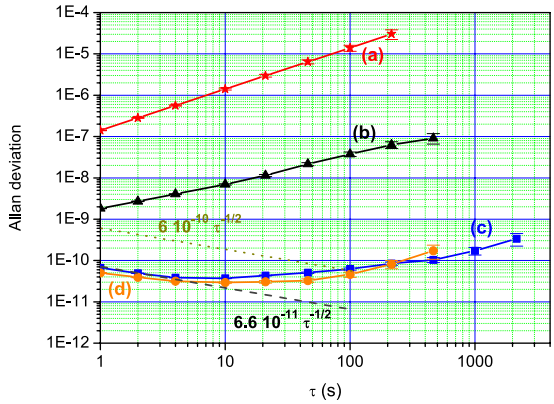


(b)

FIG. 11. Local oscillator frequency versus time (a) and corresponding Allan deviation (b). Different configurations were tested. (a) Free-running HBAR-based source without HBAR temperature control, (b) free-running HBAR-based source with HBAR temperature control, (c) HBAR-based source with HBAR temperature control and locked to the atomic transition frequency, (d) laboratory-prototype microwave synthesizer (RS SMB100A) source locked to the atomic transition frequency. The HBAR is stabilized at 68 °C. The Cs-Ne microcell temperature is 84 °C. The total laser power incident in the cell is 30 $\mu$W. The dotted line, with a slope of $6\times10^{-10}\tau^{-1/2}$, shows typical short-term frequency stability specifications of MACs. The dashed line, with a slope of $6.6\times10^{-11}\tau^{-1/2}$, is a fit for short integration times to the Allan deviation obtained with the HBAR-based local oscillator.

fractional frequency stability of the free-running HBAR-based source is measured to be $1.4 \times 10^{-7}\,\tau$ that corresponds to a typical variation of the oscillator frequency of 643 Hz/s. With HBAR temperature control, the Allan deviation of the free-running HBAR-based source is improved at the level of $1.8 \times 10^{-9}$ at 1 s and $3.7 \times 10^{-8}$ at 100 s, demonstrating an improvement factor of about 670 at $\tau = 100$ s compared to the non-temperature-stabilized regime. When locked to the atomic transition frequency, the HBAR-source exhibits a fractional frequency stability of $6.6 \times 10^{-11}\,\tau^{-1/2}$ up to 5 s, limited by the signal-to-noise ratio of the CPT signal. This measured short-term frequency stability, better than those reported in Refs. 17 and 35, is for $\tau$ up to 100 s well below the typical short-term stability specification of $6 \times 10^{-10}\,\tau^{-1/2}$ required in miniature atomic clocks. After 5 s, the clock frequency stability was found to be limited by laser power effects. At 100 s, the stabilization of the HBAR-oscillator to the atomic transition frequency allows to improve further its frequency stability by about 600 to reach the level of $6.8 \times 10^{-11}$. For comparison, a frequency stability test was performed by using as local oscillator a laboratory-prototype microwave synthesizer (RS SMB100A) driven by a 10 MHz quartz oscillator. It is observed in this case that the short-term fractional frequency stability of the clock is recorded at the level of $5 \times 10^{-11}\,\tau^{-1/2}$ up 5 s. Nevertheless, the observed difference between the two stability curves (HBAR-based source and laboratory-type synthesizer) is within the measurement errors and can be attributed to different loop settings. These results show that the performance of the HBAR-based oscillator is well suited for realizing miniature atomic clocks with excellent frequency stabilities.

## V. DISCUSSIONS

The work presented in this article is an original approach for the development of HBAR-sources dedicated to be used as local oscillators in MACs. Initially, tuning finely the output frequency of a HBAR resonator is not obvious due to the difficulty to control accurately thicknesses of materials during the fabrication process. Additionally, HBARs currently exhibit a high temperature coefficient of frequency of 10–20 ppm/°C. Techniques to reduce the HBAR temperature sensitivity exist[15] but often at the expense of a degradation of the Q-factor and supplemental technological steps bringing increased complexity. Eventually, an inherent characteristic of HBAR is their multi-mode spectrum that complicates their use in an oscillator and forces one to filter the response to select a single resonance. In this article, we tried to convert these drawbacks into strong key points to adapt the HBAR to MAC applications. The high-temperature sensitivity is an advantage for coarse tuning of the HBAR frequency and hence compensate for unreachable thickness resolutions for reaching the Cs transition frequency. Moreover, the fine tuning of the HBAR oscillator frequency with a voltage-controlled phase shifter in the loop prevents the use of a high-power consuming direct digital synthesizer. In our system, the voltage-to-frequency tuning with the VCPS was about 8 kHz/V. Then, a supply voltage with a resolution of 1 $\mu$V allows a satisfying frequency resolution of 8 mHz.

While no integration and packaging efforts were done in this work, related activities demonstrate that this strategy is compatible with low volume and low power consumption requirements for MAC applications. In terms of compacity, the dimensions of the HBAR are driven by the electrode area and the total material stack thickness. The acoustic energy confinement in the substrate requires electrodes dimensions "very" large with respect to the acoustic wavelength. Operating above 2 GHz induces wavelengths lower than 6 $\mu$m and a $1 \times 1$ mm large HBAR transducer meets the acoustic energy confinement conditions. Hence, HBAR meets clearly the compact resonator requirement. The dimensions of the oscillator circuit have not been considered in this investigation but have been demonstrated at the integrated chip level in the literature.[36]

The power consumption of the HBAR-local oscillator is mainly driven by the microwave sustaining amplifier and the resonator thermal control. The power consumption of the VCPS (capacitive load polarized with a DC voltage) is negligible. In our system, the main contribution to the consumption budget is the HBAR temperature control circuit with over 900 mW needed to heat the packaged HBAR. Such a power consumption is not acceptable for embedded applications. The best way to reduce such a large current would be to confine the heating to the bare resonator rather than the whole packaged device. Ideally, the temperature set point of the HBAR should be fixed at about 85–90 °C to support a MAC operation typical temperature range of −20 to +80 °C without using a high-power consuming Peltier element. MEMS metal oxide gas sensors, which require operating temperatures several hundreds of celsius degrees above room temperature, have met this challenge by fitting the sensing element to heat insulating hinges, patterning the sensing element with the heating coil, and confining the heating to the part of interest, in our case the volume in which the acoustic energy is stored, reaching sub-100 mW consumption to reach 300 °C for 1000 $\mu$m$^2$ large devices.[37] We think that the power consumption of a HBAR oscillator for MAC applications could be reduced at a maximum of 10–20 mW. Nevertheless, a question remains. In standard MACs, the output useful signal frequency for end-users is 10 MHz. In a potential HBAR-based oscillator Cs vapor cell MAC, the LO is frequency-stabilized at 4.596 GHz. This microwave frequency is not well-adapted for standard widespread applications. This issue would impose to use a frequency divider to downconvert the 4.596 GHz signal to about 100 or 10 MHz, adding a power consumption of 10–20 mW if dedicated components are used.[38–40]

We demonstrated that HBAR oscillators exhibit ultra-low phase noise performances. Hence, it is interesting to note that MACs using HBAR-based oscillators could allow the development of time-frequency references combining in a single device excellent phase noise and long-term frequency stability properties, opening potentially the MAC technology to a wider spectrum of applications. Up to date, the short-term fractional frequency stability of MACs is mainly limited by the laser FM noise and not by the LO intermodulation effect. Thus, to date, improving the LO noise with HBAR-based oscillators should not improve the clock short-term stability.

However, we demonstrated that the use of a HBAR-LO rejects the Dick effect contribution to a level close to the clock shot noise limit. This aspect could be of great interest in the future if new-generation high-performance MACs using miniature low-consumption lasers with ultra-narrow spectral linewidth[41] and reduced AM noise were developed.

## VI. CONCLUSIONS

We reported the design strategy and the use of a double-port AlN/Sapphire 2.298 GHz HBAR-oscillator-based 4.596 GHz frequency synthesizer devoted to be used as a local oscillator in a Cs vapor cell CPT-based atomic clock. Dedicated techniques, exploiting the HBAR temperature sensitivity for coarse frequency tuning and the use of a VCPS in the oscillator loop, were proposed to ensure the HBAR-oscillator frequency to be resonant with the half of Cs atom clock frequency (4.596 GHz). The HBAR presents a Q-factor of about 24 000 and a temperature sensitivity of −23 ppm/°C. The 4.596 GHz output signal exhibits exceptional phase noise performances of −105 dB rad$^2$/Hz at 1 kHz offset frequency, rejecting the intermodulation effect contribution to the clock short-term fractional frequency stability at the level of $4.3 \times 10^{-13}$, a value comparable to the clock quantum noise limit. A Cs microcell-based CPT clock was tested using the HBAR-source, demonstrating a clock short-term frequency stability of $6.6 \times 10^{-11}$, limited by the CPT resonance signal-to-noise ratio and not by the LO phase noise. Discussions were reported to evaluate the potential of this technology to be implemented in low-volume and low power consumption miniature atomic clocks.

## ACKNOWLEDGMENTS

This work has been funded by LabeX FIRST-TF. The HBAR was manufactured by CEA/LETI in the framework of the ORAGE RAPID project funded by the French Direction Générale de l'Armement (DGA) agency.

[1]G. Alzetta, A. Gozzini, L. Moi, and G. Orriols, Il Nuovo Cimento B Ser. **36**, 5 (1976).
[2]E. Arimondo, Prog. Opt. **35**, 257 (1996).
[3]S. Knappe, V. Shah, P. D. Schwindt, L. Hollberg, J. Kitching, L.-A. Liew, and J. Moreland, Appl. Phys. Lett. **85**, 1460 (2004).
[4]S. Knappe, in *Comprehensive Microsystems*, edited by Y. B. Gianchandani (Elsevier B, Amsterdam, 2007), Vol. 3, pp. 571–612.
[5]R. Lutwak, A. Rashed, M. Varghese, G. Tepolt, J. LeBlanc, M. Mescher, D. K. Serkland, K. M. Geib, G. M. Peake, and S. Römisch, in *39th Annual Precise Time and Time Interval (PTTI) Meeting* (Institute of Navigation, Long Beach, CA, 2007), pp. 269–281.
[6]See http://www.microsemi.com/products/timing-synchronization-systems/embedded-timing-solutions/components/sa-45s-chip-scale-atomic-clock for information on chip scale atomic clocks developed by Microsemi.
[7]A. Brannon, J. Breitbarth, and Z. Popović, in *IEEE MTT-S International Microwave Symposium Digest* (IEEE, Long Beach, CA, 2005), pp. 1535–1538.
[8]S. Römisch and R. Lutwak, in *Proceedings of IEEE International Frequency Control Symposium and Exposition* (IEEE, Miami, FL, 2006), pp. 448–451.
[9]C. Audoin, V. Candelier, and N. Dimarcq, IEEE Trans. Instrum. Meas. **40**, 121 (1991).
[10]G. J. Dick, in *Proceedings of Precise Time and Time Interval* (U.S. Naval Observatory, Redondo Beach, CA, 1987), pp. 133–147.
[11]Y. Zhao, S. Tanner, A. Casagrande, C. Affolderbach, L. Schneller, G. Mileti, and P. A. Farine, IEEE Trans. Instrum. Meas. **64**, 263 (2015).
[12]K. M. Lakin, IEEE Trans. Ultrason., Ferroelectr., Freq. Control **52**, 707 (2005).
[13]K. M. Lakin, G. R. Kline, and K. T. McCarron, IEEE Trans. Microw. Theory Tech. **41**, 2139 (1993).
[14]W. Pang, Y. Hongyu, Z. Hao, and K. E. Sok, in *IEEE MTT Symposium International Microwave Symposium Digest* (IEEE, Long Beach, CA, 2005), p. 1279.
[15]H. Yu, W. Pang, H. Zhang, and E. S. Kim, IEEE Trans. Ultrason., Ferroelectr., Freq. Control **54**, 2102 (2007).
[16]D. Gachon, E. Courjon, J. Masson, V. Petrini, J. Y. Rauch, and S. Ballandras, in *Proceedings of IEEE Ultrasonics Symposium* (IEEE, New-York, USA, 2007), p. 1417.
[17]H. Yu, C.-Y. Lee, W. Pang, H. Zhang, A. Brannon, J. Kitching, and E. S. Kim, IEEE Trans. Ultrason., Ferroelectr., Freq. Control **56**, 400 (2009).
[18]N. Chrétien, G. Martin, E. Lebrasseur, H. Wang, T. Baron, S. Ballandras, E. Henaff, F. Tomaso, and L. Chommeloux, in *Ultrasonics Symposium (IUS), 2012 IEEE International* (IEEE, 2012), pp. 2210–2213.
[19]A. Reinhardt, M. Delaye, J. Abergel, V. Kovacova, M. Allain, L. Andreutti, D. Mercier, J. Georges, F. Tomaso, and P. Lassagne, in *Ultrasonics Symposium (IUS), 2013 IEEE International* (IEEE, 2013), pp. 1922–1925.
[20]V. B. Braginsky, V. S. H. Chenko, and K. S. Bagdassarov, Phys. Lett. A **120**, 300 (1987).
[21]N. Chrétien, "Electronics dedicated to oscillators and physical measurement using elastic wave sensors," Ph.D. thesis, Université de Franche-Comté, 2014 in French.
[22]C. C. Ruppel and T. A. Fjeldly, *Advances in Surface Acoustic Wave Technology, Systems and Applications* (World Scientific, 2000), Vol. 1.
[23]R. Boudot, C. Rocher, N. Bazin, S. Galliou, and V. Giordano, Rev. Sci. Instrum. **76**, 095110 (2005).
[24]B. François, C. Calosso, M. A. Hafiz, S. Micalizio, and R. Boudot, Rev. Sci. Instrum. **86**, 094707 (2015).
[25]D. B. Leeson, Proc. IEEE **54**, 329 (1966).
[26]S. Gribaldo, C. Chay, É. Tournier, and O. Llopis, IEEE Trans. Ultrason., Ferroelectr., Freq. Control **53**, 1982 (2006).
[27]E. S. Ferre-Pikal, M. C. D. Arámburo, F. L. Walls, and K. M. Lakin, IEEE Trans. Ultrason., Ferroelectr., Freq. Control **48**, 506 (2001).
[28]D. S. Bailey, M. M. Driscoll, R. Jelen, B. R. McAvoy *et al.*, IEEE Trans. Ultrason., Ferroelectr., Freq. Control **39**, 780 (1992).
[29]V. Shah and J. Kitching, in *Advances in Atomic, Molecular and Optical Physics*, edited by E. Arimondo, P. R. Berman, and C. C. Lin (Elsevier, Amsterdam, 2010), Vol. 59, Chap. 2.
[30]A. Al-Samaneh, M. B. Sanayeh, M. Miah, W. Schwarz, D. Wahl, A. Kern, and R. Michalzik, Appl. Phys. Lett. **101**, 171104 (2012).
[31]F. Gruet, A. Al-Samaneh, E. Kroemer, L. Bimboes, D. Miletic, C. Affolderbach, D. Wahl, R. Boudot, G. Mileti, and R. Michalzik, Opt. Express **21**, 5781 (2013).
[32]M. Hasegawa, R. Chutani, C. Gorecki, R. Boudot, P. Dziuban, V. Giordano, S. Clatot, and L. Mauri, Sens. Actuators, A **167**, 594 (2011).
[33]R. H. Dicke, Phys. Rev. **89**, 472 (1953).
[34]G. A. Pitz, D. E. Wertepny, and G. P. Perram, Phys. Rev. A **80**, 062718 (2009).
[35]R. Boudot, M. Li, V. Giordano, N. Rolland, P. Rolland, and P. Vincent, Rev. Sci. Instrum. **82**, 034706 (2011).
[36]A. Hajimiri and T. H. Lee, *The Design of Low Noise Oscillators* (Springer Science & Business Media, 1999).
[37]D. Briand, "Micromachined semiconductor gas sensors," in *Semiconductor Gas Sensors*, edited by R. Jaanso and O. Kiang Tan (Woodhead Publishing series in Electronic and Optical Materials, 2013).
[38]B. Razavi, K. F. Lee, and R. H. Yan, IEEE J. Solid-State Circuits **30**, 101 (1995).
[39]G. Haijun, S. Lingling, C. Chaobo, and Z. Haiting, J. Semicond. **33**, 115004 (2012).
[40]A. Felder, J. Hauenschild, R. Mahnkopf, and H. Rein, in *Bipolar/BiCMOS Circuits and Technology Meeting, 1992, Proceedings of the 1992* (IEEE, 1992), pp. 159–162.
[41]F. M. di Sopra, H. P. Zappe, M. Moser, R. Hövel, H.-P. Gauggel, and K. Gulden, IEEE Photonics Technol. Lett. **11**, 1533 (1999).